GA–A22704

# PHYSICS OF ADVANCED TOKAMAKS

by
T.S. TAYLOR

NOVEMBER 1997

## DISCLAIMER

**GA–A22704**

# PHYSICS OF ADVANCED TOKAMAKS

**by**
**T.S. TAYLOR**

**This is a preprint of an invited paper to be presented at the 24th European Conference on Controlled Fusion and Plasma Physics, June 9–14, 1997, Berchtesgaden, Germany and to be published in *Plasma Physics & Controlled Fusion*.**

**Work supported by**
**the U.S. Department of Energy**
**under Contract Nos. DE-AC03-89ER51114, W-7405-ENG-48,**
**DE-AC05-96OR22464, DE-AC02-76CH03073 and**
**Grant Nos. DE-FG02-89ER53297, DE-FG02-91ER54109,**
**and DE-FG03-86ER53266**

**GA PROJECT 3466**
**NOVEMBER 1997**

# Physics of advanced tokamaks

**T.S. Taylor**

General Atomics, P.O. Box 85608, San Diego, California 92186-5608

**Abstract.** Significant reductions in the size and cost of a fusion power plant core can be realized if simultaneous improvements in the energy replacement time, $\tau_E$, and the plasma pressure or beta, $\beta_T = 2\ \mu_0 <P>/B^2$ can be achieved in steady-state conditions with high self-driven, bootstrap current fraction. Significant recent progress has been made in experimentally achieving these high performance regimes and in developing a theoretical understanding of the underlying physics. Three operational scenarios have demonstrated potential for steady state high performance, the radiative improved (RI) mode, the high internal inductance or high $\ell_i$ scenario, and the negative central magnetic shear, NCS (or reversed shear, RS) scenario. In a large number of tokamaks, reduced ion thermal transport to near neoclassical values, and reduced particle transport have been observed in the region of negative or very low magnetic shear: the transport reduction is consistent with stabilization of microturbulence by sheared E×B flow. There is strong temporal and spatial correlation between the increased sheared E×B flow, the reduction in the measured turbulence, and the reduction in transport. The DIII–D tokamak, the JET tokamak and the JT–60U tokamak have all observed significant increases in plasma performance in the NCS operational regime. Strong plasma shaping and broad pressure profiles, provided by the H–mode edge, allow high beta operation, consistent with theoretical predictions; and normalized beta values up to $\beta_T/(I/aB) \equiv \beta_N \sim 4.5$%-m-T/MA simultaneously with confinement enhancement over L–mode scaling, $H = \tau/\tau_{ITER-89P} \sim 4$, have been achieved in the DIII–D tokamak. In the JT–60U tokamak, deuterium discharges with negative central magnetic shear, NCS, have reached equivalent break-even conditions, $Q_{DT}$ (equiv) = 1.

## I. Introduction

The viability of a tokamak as an economically and environmentally attractive power plant requires both sufficient energy confinement time, $\tau_E$, for ignition margin, and sufficient volume average toroidal beta, $\beta_T = 2\mu_0 \langle p \rangle / B_T^2$, for adequate fusion power density. Here, $\langle p \rangle$ is the volume average pressure, and $B_T$ is the magnitude of the vacuum toroidal magnetic field at the center of the last closed flux surface. In many tokamak power plant designs, the conditions necessary for ignition are gained primarily by increasing the plasma current: energy confinement and maximum achievable beta are found to scale approximately linearly with plasma current, $I_P$; $\tau_E \propto I_P$, and $\beta_T^{max} = \beta_N I_P/aB_T$ (Troyon 1984). However, common confinement scalings such as the ITER–89P (Yushmanov 1990) result in large tokamak core designs. Higher energy confinement operational modes were discovered on ASDEX and subsequently on many other tokamaks. This new high confinement mode, H–mode, is characterized by a steep gradient region near the plasma boundary and energy confinement enhancement, H, $H \equiv \tau_E/\tau_{ITER-89P} \approx 2$ (Groebner 1993). Tokamak designs with $H \gtrsim 2$, and $\beta_N \leq 2.5$ (such as ITER) are now envisioned. More recently, many short pulse experiments are routinely observing confinement times which far exceed that predicted by the ITER–89 low energy confinement mode, L–mode, scaling, with H = 3–4. In addition high values of normalized beta, $\beta_N$ = 4–6, have been observed in some cases. If this factor of 2 increase in H and $\beta_N$ over nominal H–modes could be obtained simultaneously and in long pulse near steady state conditions, an approximate factor of two reduction in size, capital cost, and cost of electricity for a tokamak fusion power plant could be gained (Galambos 1995, Goldston 1994, Kikuchi 1994, Jardin 1997).

The study of tokamak operational scenarios with the potential of simultaneous increase in the confinement enhancement and normalized beta in near steady state conditions has recently become known as "Advanced Tokamak" research. The goals of such research are regimes with H significantly greater than 2 (approaching 4) and $\beta_N$ significantly greater than 3 (approaching 5%-m-T/MA), with little or no externally driven current, $E_\phi(\rho) \rightarrow 0$. Furthermore, maintaining such conditions with self-consistent heat removal, He

ash removal, and impurity and density control is necessary. It should be pointed out that the requirement for steady state conditions is not relieved for pulsed tokamak power plant designs, since these designs require very high availability, which in turn requires very long pulse lengths and minimum time between pulses.

The requirement of both high fusion power density and near steady-state operation increase the need to operate at high $\beta_N$. High gain steady-state operation requires significant self-driven bootstrap current fraction, $f_{BS} = I_{BS}/I_P \propto \varepsilon^{1/2}\,\beta_P \propto C_{BS}\,\beta_N\,q/\varepsilon^{1./2}$ . The coefficient $C_{BS}$ is dependent on the details of the internal profiles and to a lesser extent on the plasma cross section shape; q is the cylindrical approximation to the safety factor; and $\varepsilon$ is the inverse aspect ratio, a/R, a being the minor radius, and R the major radius. The fusion power density increases with increasing $\beta_T$ the current drive power decreases with increasing $f_{BS}$ and increasing $\beta_P$. This need for both high $\beta_T$ and $\beta_P$ leads to high $\beta_N$, since $\beta_T^*\,\beta_P = \beta_N^2\,(1+\kappa^2)/8$ where $\kappa$ is the discharge elongation. This is shown graphically in Fig. 1: the region for "advanced tokamaks" is toward the upper right hand corner.

The path to these advanced tokamak regimes is the plasma cross sectional shape and the control of the internal profiles (Taylor 1994). These profiles include: the current density profile, $\langle J(\rho)\rangle$, or safety factor profile, q(ρ); the pressure profile, p(ρ); the rotation profile, V(ρ); the density profile, n(ρ); and the impurity, Z(ρ), or the radiation profile $P_{rad}(\rho)$. Whereas the more standard tokamak approach largely involves 0-d scaling, advanced tokamak research is inherently a 1–2 dimensional problem. Only recently, has the diagnostic capability become available to adequately measure the temporal evolution of these profiles, necessary for developing a physics understanding of the enhanced performance. Especially important has been the recent capability to measure the internal field pitch and determine the details of the q profile and current density profile (Wróblewski 1993, Rice 1995, Levington 1989, Soltwisch 1986, O'Rourke 1991).

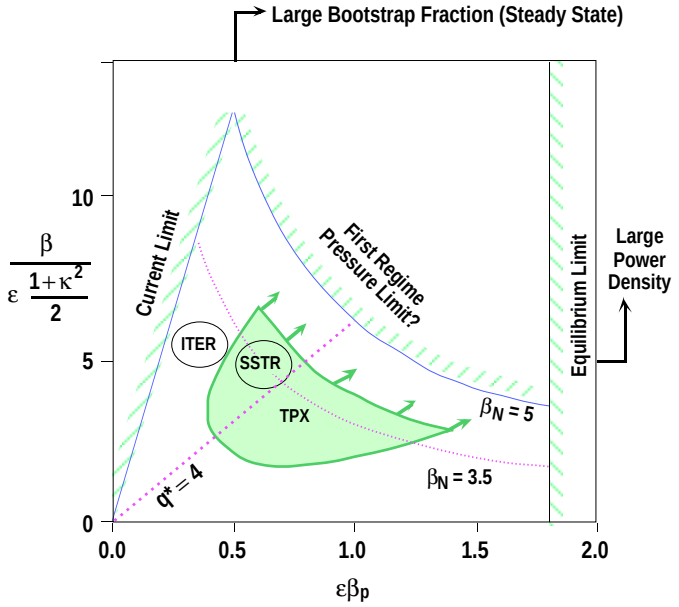


Fig. 1. A compact steady-state tokamak requires operation at high $\beta_N$. Advanced tokamak operation is toward the upper right hand corner, high $\beta_N$.

Significant progress has been made recently theoretically, in modeling, and experimentally, in understanding the physics of advanced tokamak operational modes. This manuscript is a review of that recent progress. In Section II, we discuss the several advanced operational scenarios that are being actively investigated, with a focus on the negative central magnetic shear (NCS) or reversed shear (RS) regime. The present understanding of the reduction in transport and increased confinement is given in Section III. The physics understanding of the beta limit, the connection between the plasma cross section and the pressure profile, and the role of wall stabilization are presented in Section IV. Some discussion of the self-driven bootstrap current, the alignment of the bootstrap current and progress toward steady state is discussed in Section V. In Section VI is our summary discussion.

## II. Advanced Tokamak Opertional Scenarios

There are a number of operational scenarios that have been identified that have the potential for steady-state high confinement, high beta operation. We will briefly discuss three of these operational scenarios; (1) the radiative I–mode, (2) the high $\ell_i$ regime, and (3) the negative central magnetic shear regime. The NCS regime, RS regime, and the optimized shear regime are for practical purposes indistinguishable and all characterized by negative or very low central magnetic shear and reduced internal transport. There has been significant emphasis and progress in these operational regimes recently. The details of the profiles play an important aspect in the formation of these discharges and in the physics understanding of the improved confinement and stability limits. In the case of the RI–mode, it is the magnitude and the profile of the radiation that plays the key in obtaining this regime. In both the high $\ell_i$ and NCS regime, it is the evolution of the current profile that is the key in establishing the regimes. The current density profile plays a unique role in the high $\ell_i$ and NCS because it is the profile that is actively modified to achieve the regimes and because it is

important in understanding the physics. The details of other profiles; such as the pressure, the density, and the rotation profiles, are also key to understanding the physics of the NCS regime.

The impact of the current profile in the high $\ell_i$ and NCS regimes is motivated by theoretical work which indicates a stabilizing effect from magnetic shear on both ideal high n ballooning modes and electrostatic microinstabilities. In Fig. 2(a) is shown schematically the ideal ballooning stability. At high magnetic shear, $s = \rho/q\ dq/d\rho$ the maximum stable pressure gradient limited by ballooning modes increases significantly, almost linearly with increasing shear (Wesson 1985). At low magnetic shear, the unstable region disappears entirely and there is no limit to the pressure gradient. As shown in Fig. 2(b), the growth rate for trapped particle modes decreases both at higher magnetic shear and lower magnetic shear (Waltz 1993). From these two dependencies, one might expect tokamak performance might be improved by either an increase in the magnetic shear over a substantial portion of the plasma or a decrease of the magnetic shear over a substantial portion of the plasma.

The qualitative feature of the current profiles that are required to produce high positive shear and low or negative shear are seen by the large aspect ratio cylindrical relation between the magnetic shear and the current density: $s(\rho) \approx [J(0)\ q(0) - J(\rho)\ q(\rho)]/J(0)\ q(0)$, where $\rho$ is the reduced radial coordinate, J and q are the current density and safety factor, and s is the magnetic shear. High positive shear is obtained in the outer portion of the plasma when plasma current flows primarily in the core of the plasma and is very small (or negative) in the outer portion of the plasma. Since this current distribution gives a high internal inductance, $\ell_i$, this scenario is known as high $\ell_i$: $\ell_i = 1/V \int dV\ B_\theta^2 / B_\theta^2(\text{ave})$, where $B_\theta(\text{ave}) = \mu_0 I_P/C_P$, is the average poloidal magnetic field on the last closed flux surface: $I_P$ is the enclosed plasma current and $C_P$ is the poloidal circumference. Low magnetic shear, or negative magnetic shear can be obtained in the core of the plasma when the current density flows primarily in the outer portion of the plasma, and remains lower in the center of the plasma: $J(0)\ q(0) << J(\rho)\ q(\rho)$. The NCS regime is also referred to reverse shear (RS), since in these plasmas the shear changes from negative to positive from the center outward: the standard current profile distribution has a monotonically increasing q profile, or positive shear across the entire plasma.

## *2.1. Radiative I–mode*

The radiative I-mode holds the promise of a regime that can maintain high confinement at very high densities, approaching or exceeding the Greenwald density limit (Greenwald 1988), and with the major portion of the plasma energy radiated from the plasma periphery. These characteristics make this operational scenario easily compatible with power exhaust. This regime has been identified and evaluated quite extensively by the TEXTOR group (Messiaen 1997, Messiaen 1996, Wolf 1996). The improvement in confinement is observed in neutral beam injection (NBI) and ion cyclotron resonance frequency (ICRF) heated discharges with impurity seeding, usually neon, and is similar to the Z–mode observed in ISXB (Lazarus 1985). A typical RI–mode discharge is shown in Fig. 3. As is shown the confinement increases with the injection of neon. The total stored energy is kept constant by feedback control on the input power, and the radiative fraction is controlled by feedback on the neon injection. The confinement exceeds that predicted by the ITERH93–P scaling (reference) and increases with density, even beyond the Greenwald density limit. The energy confinement scaling in this operational scenario is well represented by $\tau_{RI} = (n_e/n_{e,GR})\ \tau_{ITERH93-P}$, clearly indicating the favorable density dependence.

The physics mechanisms responsible for the improved confinement are not yet well understood for the RI–mode, but there are several that are being further evaluated: (i) a modest increase in the density peaking, (ii) a peaking of the current density profile, (iii) increase in the toroidal velocity, and (iv) a decrease in the edge electron temperature and associated increase in the particle confinement time (Messiaen 1997). The stability limit in the TEXTOR RI–modes are similar to those observed in other TEXTOR discharges, $\beta_N \leq 2$. It remains to be seen whether the confinement improvement and further increases in the stability limit

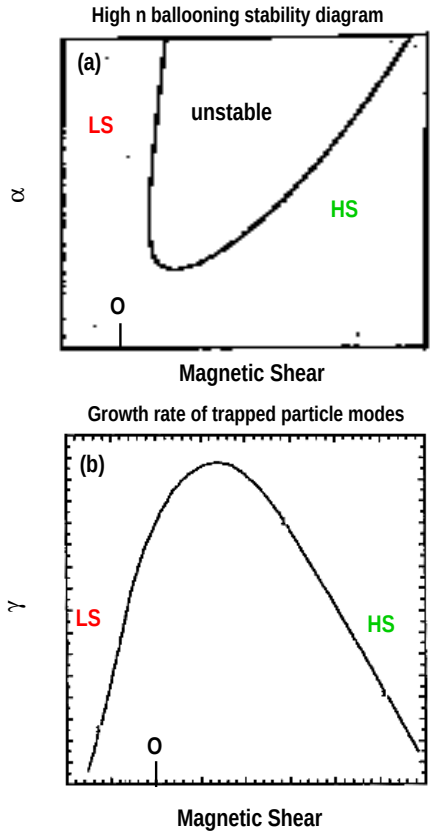


Fig. 2. Both low magnetic shear (LS) and high shear (HS) are favorable for: (a) reduced turbulence and reduced transport, (b) higher beta. Magnetic shear is $s \propto (r/q)\ dq/dr$; normalized pressure gradient, $\alpha \propto R/B_T^2\ q^2\ d\rho/dr$.

can be realized in large tokamaks, and in strongly shaped tokamaks: recent TFTR RI–mode results indicate improvement in the confinement, and RI–mode experiments are planned for DIII–D.

## *2.2. High $\ell_i$*

Both $\tau_E$ and $\beta_T^{max}$ have been shown to increase with increasing internal inductance $\ell_i$, which would appear to make the high $\ell_i$ scenario a very attractive scenario for advanced tokamak performance. However, the ability to maintain the high $\ell_i$, consistent with significant bootstrap current, creates a challenge. High $\ell_i$ plasmas are created by negative plasma current ramps (Zarnstorff 1993, Ferron 1993, Kamada 1994), and by rapidly increasing plasma volume by elongation ramps (Lao 1993) and by expanding the minor radius (Sabbagh 1996). Creating high $\ell_i$ by radial expansion has allowed the formation of TFTR discharges with $I_P$ up to 2.3 MA and $\ell_i$ up to 1.5. In such plasmas the a D-T fusion power of up to 8.7 MW was obtained, no longer limited by MHD stability but limited by the ability of the limiter to handle the power (Sabbagh 1996).

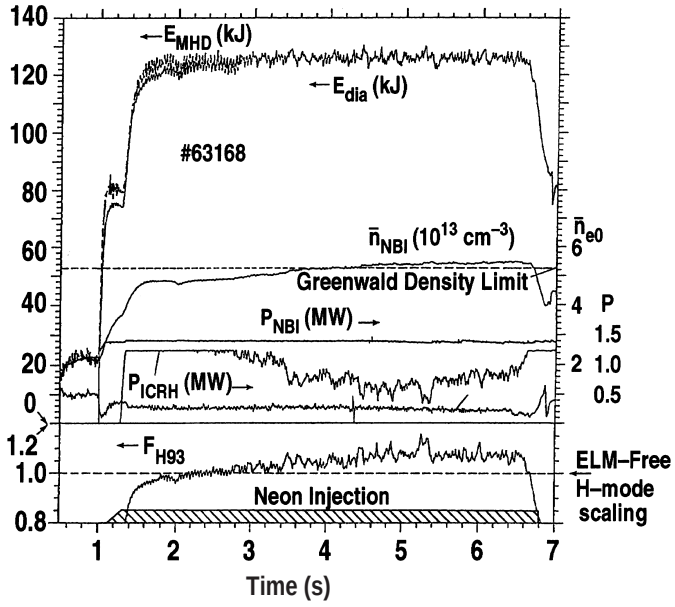


Fig. 3. Radiative I–mode: A.M. Messiaen Phys. Plasmas **4**, 1690 (1997).

The increase in confinement with increasing $\ell_i$ is observed in both H–mode and L–mode plasmas and irrespective if the high $\ell_i$ is created by rapidly reducing the plasma current or by increasing the plasma volume (Ferron 1993): the energy confinement enhancement increases with $\ell_i$; $H \propto \ell_i$. The maximum achievable beta also has been shown to increase with $\ell_i$, $\beta_T^{max} \approx 4\ \ell_i\ I_P/aB_T$, under a variety of conditions consistent with MHD theory and numerical calculations (Strait 1994, Taylor 1991, Taylor 1993, Ferron 1993, Lao 1992, Kessner 1993, Kamada 1994, Kamada 1996).

The above techniques to produce high $\ell_i$ are presently transient in nature. When the current profile becomes fully relaxed, with predominantly ohmic drive plus the bootstrap current, the $\ell_i$ becomes reduced and the confinement and stability limit are also reduced. This decrease in $\ell_i$ is a consequence of the radial distribution of the bootstrap current. The bootstrap current density is proportional to $\varepsilon^{1/2}\ p'$, and so the "natural" profile of the bootstrap current is a hollow current, even for peaked pressure profiles. In the high $\ell_i$ discharges, it is the region near the boundary where the magnetic shear is high, the transport is reduced and the pressure gradient is high. At high $\beta$ fully relaxed profiles will include a hollow bootstrap current which is high near the plasma edge, reducing the attainable $\ell_i$. High triangularity, $\delta = 0.7$, and highly elongated, $\kappa = 1.8$, equilibria, self-consistent steady-state scenarios can be found with q near 8, $\beta_N \approx 4$ , and $\ell_i \approx 1.2$ as shown in Fig. 4. These Gedanken equilibria have ≈60% bootstrap driven current, and the pressure gradient is near the ballooning limit across the plasma cross section. The total current is the seed current in the center and the bootstrap current near the edge. Notice the relatively high edge bootstrap. $\ell_i \approx 1.4$–$1.6$ can be obtained if q(0) can be reduced to 0.55, but the impact of such low q(0) on the stability limit is not known (Lin-Liu 1995).

The attractiveness of a steady-state high $\ell_i$ scenario is somewhat questionable because of the relatively high q (low $I_P$) and modest values of $\ell_i$. However, we believe it is worth pursuing as an option for a number of reasons. (1) The high $\ell_i$ scenario is fully compatible with the RI–mode, and the high edge radiation and low edge temperature might reduce the edge bootstrap, helping maintain the high $\ell_i$. (2) The on-axis current drive is more efficient because of the higher temperature and absence of particle trapping. (3) The high $\ell_i$ mode seems to be very robust, having been obtained in L–mode and H–mode and under a variety of shapes. (4) The improvement with high $\ell_i$ appears to have no threshold in input power, density, etc. (5) Normalized beta values up to 4 are calculated to be stable without wall stabilization.

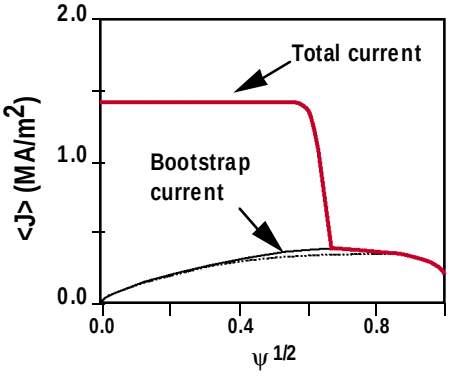


Fig. 4. Self-consistent current profile from high $\beta$, high $\ell_i$ equilibrium $\beta_N$ =4, $\ell_i$ = 1.2, $q_{95}$ = 8, $q_0$ = 1.05.

## *2.3. Negative central magnetic shear (NCS/RS/optimized shear)*

Steady-state advanced tokamak scenarios will necessarily have a high bootstrap fraction; an unavoidable consequence of very high beta, and an attractive feature that can reduce the required current drive power. Since the "natural" profile of the bootstrap current is a hollow current profile, it becomes natural to ask what is the performance potential for such profiles. The NCS/RS regime combines high confinement, potentially high beta limits with wall stabilization, high bootstrap fraction with well-aligned bootstrap current (Turnbull 1995, Kessel 1994). With increased emphasis around the world in progress toward steady-state high performance scenarios, for example in the TPX design studies (Goldston 1994, Davidson 1995), and the DIII–D advanced tokamak program (Simonen 1992, Taylor 1994); there has been renewed interest in the NCS regime. In the past three years there has been a significant amount of research addressing the NCS/RS/optimized shear regime, and significant progress in the physics understanding has been obtained in the areas of transport and stability limits.

The potential for reduced transport and improved stability limits was demonstrated in two early observations of NCS discharges. In Fig. 5(a), is shown a DIII–D high beta discharge in which the negative shear region was created by current ramp and elongation ramp during beam heating (Lazarus 1992). The central beta was determined to be 44% and the pressure gradient significantly exceeded the first regime limit: the core region was in the transition region between the first and second regime, where no unstable pressure gradient is calculated. In Fig. 5(b) is shown the JET PEP mode (Hugon 1992) which was produced by central pellet injection followed by ICRF heating. In this type of discharge, strong peaking of the pressure was observed and the effective diffusivity was decreased in the core, Fig. 5(b). In both examples shown, with a reversed negative shear region in the center: the q profile was not directly measured but was inferred from low order rational MHD observed in these discharges just prior to the collapse of the high performance phase and from large Shafranov shift of the magnetic axis. A number of facilities have recently added the capability to accurately measure the internal q profile evolution, and this has made possible systematic study of the production and performance of NCS regimes (Rice 1996a, 1996b, 1996c; Levinton 1995; Fujita 1997a, 1997b).

The most often used technique to establish the required current profile and q profile is the application of auxiliary heating during the current ramp up phase. A example of a typical DIII–D discharge evolution is shown in Fig. 6, comparing the q profile evolution with and without heating during the current ramp. Just following the plasma breakdown, q is every where very high. Auxiliary heating during the current drive phase tends to "freeze" in the current, driving the toroidal electric field near zero on axis. The applied electric field during the current ramp, drives a current that is then a maximum off axis (Rice 1996b). The different q profiles shown are those with and without the early beam heating. The bootstrap current, with a maximum off axis, can contribute to hollow current profile, especially in the early low current moderately high $\beta_P$ phase. With ohmic current drive only, the profile slowly diffuses to a profile peaked on axis with a monotonic q profile. The magnitude of the magnetic shear reversal can be controlled by the magnitude and timing of the auxiliary heating, the target density, and the delay in the plasma flattop until the time of interest, generally when additional heating is applied. Experiments in TFTR (Levinton 1996), JT–60U (Fujita 1996), and JET (Soldner

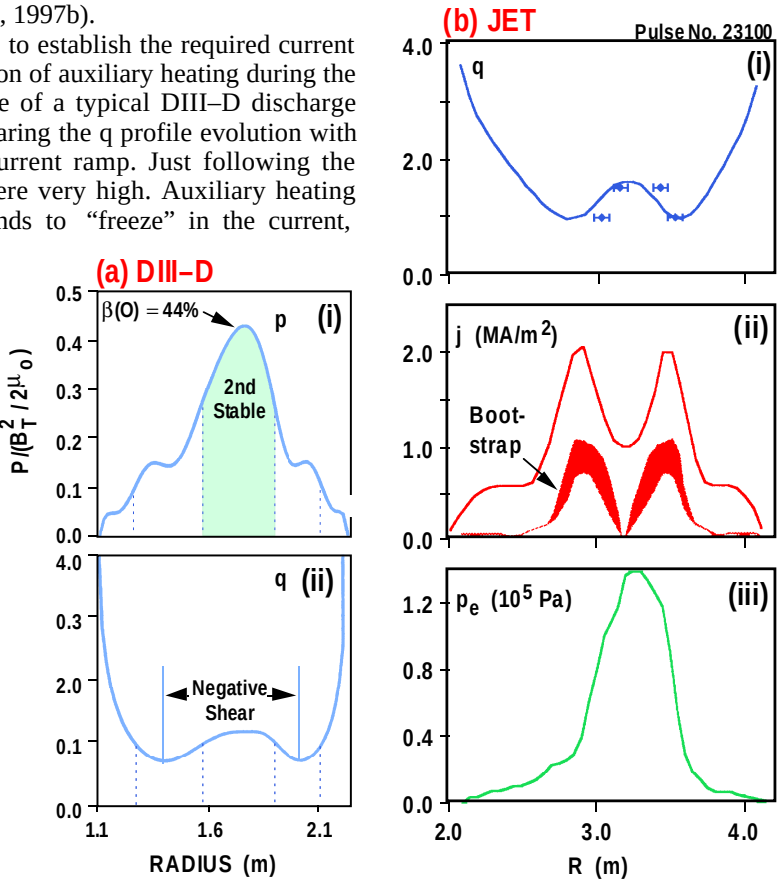


Fig. 5. Early experimental results showed (a) high beta [E.A. Lazarus, Phys. Fluids (1992)] i) pressure profile, ii) q profile; and (b) reduced transport with negative central shear [M. Hugon, Nucl. Fusion (1992)] i) q profile, ii) total current and bootstrap current profile, iii) pressure profile.

1997, Gormezano 1997) use the same early heating technique to obtain the negative shear profiles. An exception to this technique is that used in Tore Supra, where the hollow q profiles are produced by applying lower hybrid current drive (LHCD), which is absorbed and provides current drive off axis (Litaudon 1996a, 1996b). This example illustrates that the NCS regime can be established and maintained with off-axis current drive, consistent with steady state. Off axis LHCD has been shown to maintain the NCS q profile in near steady state in Tore Supra and JT–60U, and has been used during the current ramp in JT–60U and JET to establish the NCS profiles

Peaking of the profiles, indicative of an internal transport barrier (ITB), is observed in NCS/RS/ optimized shear discharges. This internal barrier is sometimes observed in the ion temperature, in the electron density, sometimes in the electron temperature, and sometimes in all three. An example of the ITB observed in all three profiles is shown in Fig. 7 from JT–60U (Fujita 1996, Koide 1997). For discharges with no edge transport barrier, the steep gradient region is located at or inside the minimum in q, $q_{min}$. The barrier is also generally observed in all three channels in JET optimized shear discharges. In TFTR, the internal transport barrier is most easily observed in the electron density, although the particle and ion transport at the barrier and inside is near neoclassical values (Levinton 1995, Synakowski 1997b). In DIII–D NCS discharges the internal transport barrier is observed clearly in the ion temperature and toroidal rotation profiles. With an increase in power, and strong negative central shear, a clear barrier is seen in the electron density, and sometimes a modest reduction in electron transport (factor of 2 to 5) is calculated (Strait 1995b; Rice 1996a, 1996c; Lao 1996; Greenfield 1997; Schissel 1997). In Tore Supra LH heated discharges, the transport barrier is seen very clearly in the electron temperature only, with a decrease of almost two orders of magnitude in the central electron transport (Litandon 1996c).

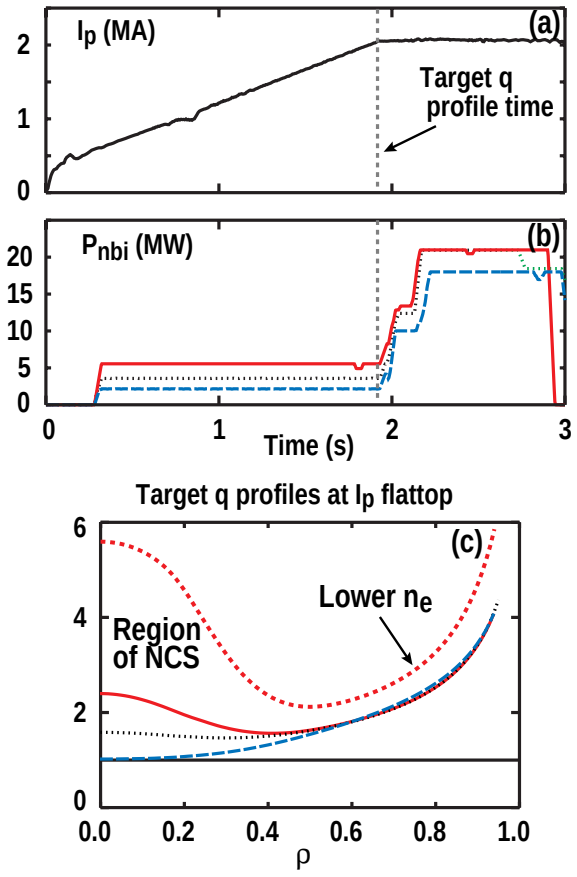


Fig. 6. NCS is reproducibly obtained with auxiliary heating during the current ramp. Shown are typical (a) plasma current (b) auxiliary heating, and (c) q-profiles (Rice, Plasma Phys. and Contr. Fusion 38, 869 (1996)).

The manifestations of the transport barrier in the different channels may be a consequence of the wide range of q profiles produced, and the species being heated. In NBI-heated discharges, there is always a reduction in ion thermal diffusivity. A reduction in the other transport channels is not always observed. In JT–60U (Koide 1997), the appearance of the transport barrier in the electrons is clearly related to the q profile, the electron ITB being observed only with strong negative magnetic shear, and not observed in discharges with weak shear, or in high beta poloidal cases with positive shear (Fig. 8). It should be pointed out that power threshold for the ITB also increases as the shear goes from more negative to less negative and positive (Fujita 1996, Synakowski 1997b).

## III. Transport

The leading paradigm to explain the reduction of transport at the internal transport barrier is E×B sheared flow stabilization of microturbulence. When there is a strong gradient in the E×B flow, the eddies (turbulence), which normally have finite radial extent, are shorn apart, greatly reducing the transport. When the shearing rate, $\omega_{E\times B}$, exceeds the decorrelation rate, $\omega_D$, the instabilities can become completely stabilized. In linear theory, the decorrelation rate can be approximated by the maximum linear growth rate, $\gamma_{lin}^{max}$ (Waltz 1995). The stabilization of microturbulence by E×B sheared flow is consistent with reduced edge transport observed in H–mode, reduced transport observed in VH–mode and high $\ell_i$, and the reduced core transport observed in NCS/ERS discharges (Burrell 1997; Lao 1996; La Haye 1995; Synakowski 1997a; 1997b; Beer 1997). Although the experimental observations are generally consistent with this paradigm, a

number of questions remain which indicate additional physics mechanisms are important or the need for more complete fully non-linear treatment of microturbulence stabilization by sheared flow.

In the NCS/ERS/optimized shear discharges, there is a synergism between the MHD stability and the E×B stabilization of microturbulence. With $q > 1$ everywhere there is no longer any drive for the m/n = 1/1 sawtooth instability. In addition with $q' \lesssim 0$, the ideal MHD ballooning modes are stable and there is no limit to the pressure gradient. Also in the $q' < 0$ regime there is no drive for neoclassical tearing modes which limit beta in long pulse discharges with standard q profiles (monotonic q) (Sauter 1997). The absence of the a pressure gradient limit is important for two reasons. First, the experimentally measured gradients exceed the first regime limit, and the improved core performance depends on achieving these high values. Secondly, the pressure gradient contributes to the radial electric field and to the Shafranov shift which leads to the stabilization of microturbulence.

There are a number of observations that strongly support the E×B shear stabilization of microturbulence. First, there is a spatial correlation between the region where $\omega_{E\times B} > \gamma_{lin}^{max}$ and the region of reduced transport as is illustrated in Fig. 9 (Lao 1996; Rice 1996; Levinton 1996; Rewoldt 1996, 1997; Schissel 1996; Greenfield 1997; Burrell 1997). It is also noted by a number of authors, that modeling of the transport by gyrokinetic and gyrofluid calculations can reproduce the observed temperature profiles, but only if the sheared E×B flow is included (Waltz 1996). In DIII–D H–mode discharges with negative or weak central magnetic shear, the ion thermal transport is observed to be near neoclassical values across the entire discharge cross section (Lao 1996; Lazarus 1996a, 1997b; Greenfield 1997) and in these discharges, $\omega_{E\times B} > \gamma_{lin}^{max}$, across the same region, the entire discharge, as shown in Fig. 10. Secondly, there is temporal correlation between the reduced transport and $\omega_{E\times B} > \gamma_{lin}^{max}$. This correla-

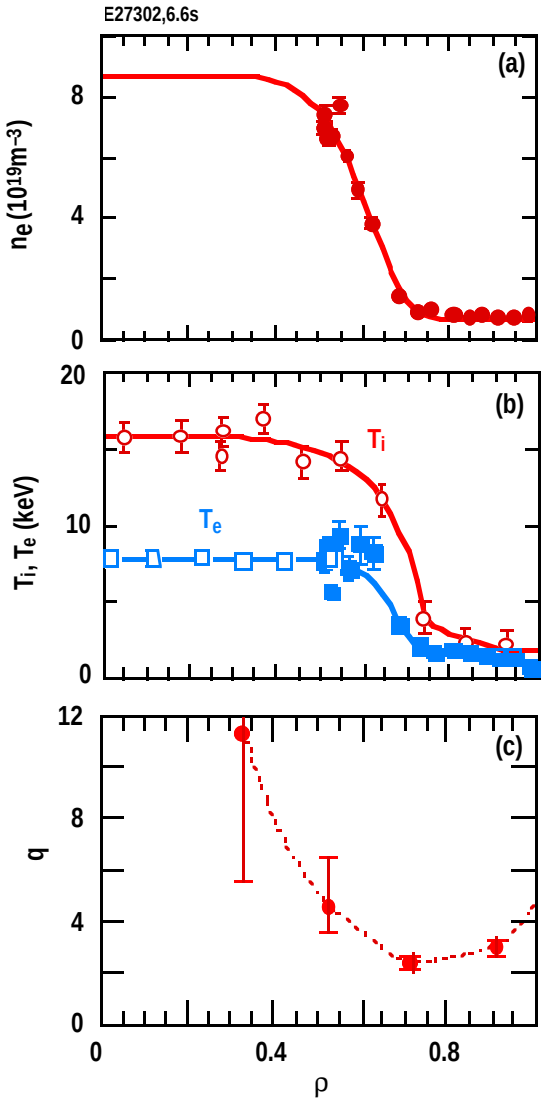


Fig. 7. An internal transport barrier (ITB) is observed near the minimum in q (JT–60U (Fujita, IAEA 1996)). (a) Electron density, $\bar{n}_e$, (b) ion and electron temperatures, $T_i$ and $T_e$, (c) q profile.

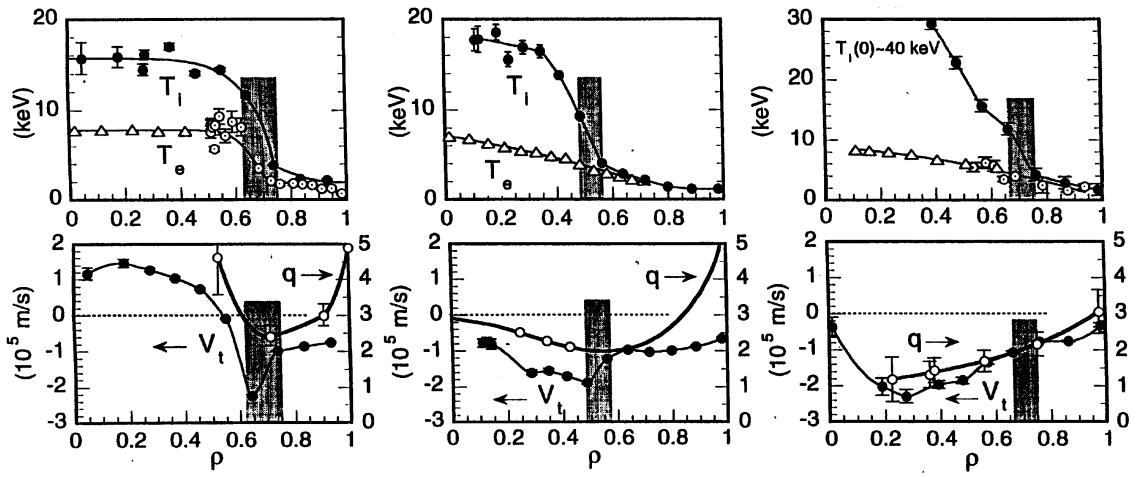


Fig. 8. The profiles in which the ITB is observed is affected by the extent of the shear reversal (Koide 1997); (a) strongly reversed (b) weakly reversed, (c) monotonic.

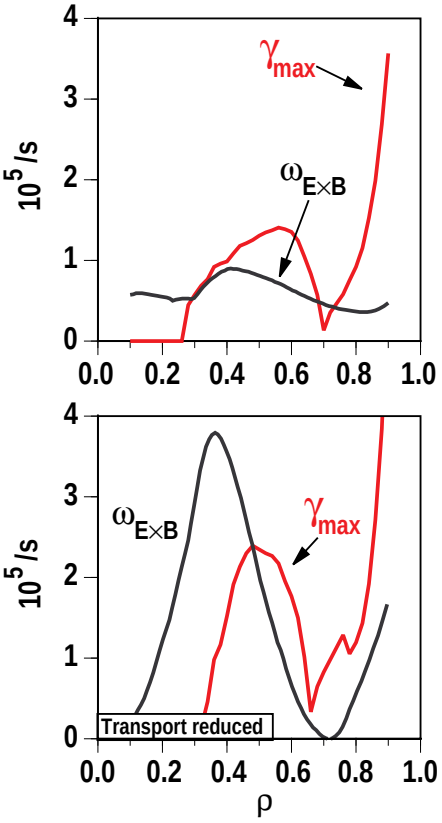


Fig. 9. The region of improved confinement is correlated with strong E×B shearing damping (a) before formation and (b) after formation (Schissel 1996, Waltz 1996), $\omega_{E\times B}$ = E×B shearing rate, $\gamma_{max}$ = ITG growth rate.

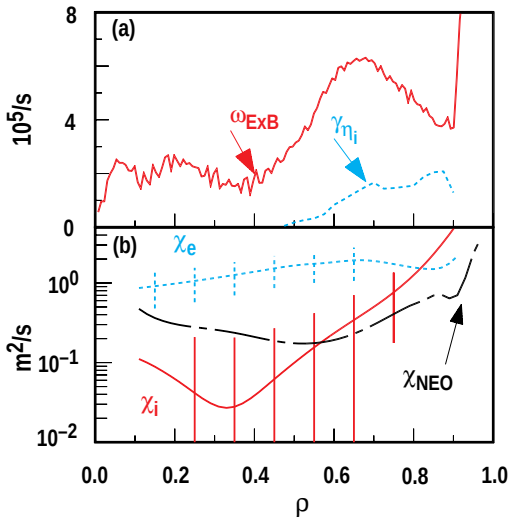


Fig. 10. In weak shear H–mode discharges in DIII–D, (a) $\omega_{E\times B} > \gamma$ and (b) $\chi_i$ approaches ion neoclassical over the entire discharge. $\beta_N = 4.5$ and H = 4 for this discharge.

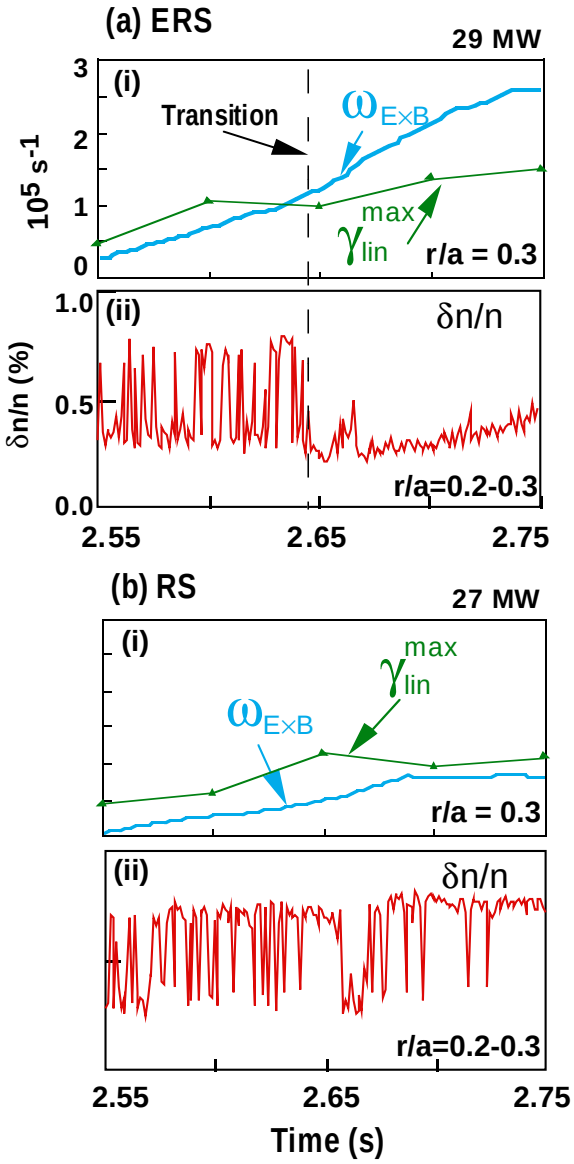


Fig. 11. E×B shearing rate exceeds the linear growth rate at the ERS transition: (a) $P_{NBI}$ = 29 MW i) $\omega_{E\times B}$ and $\gamma_{max}$ ii) density fluctuations δn/n; (b) $P_{NBI}$ = 27, no transition i) $\omega_{E\times B}$ and $\gamma_{max}$ (Synakowski 1997b).

tion is shown in Fig. 11(a), where the maximum linear growth rate and the E×B shearing rate are plotted for a TFTR discharge, and it is seen at the time of the transition the shearing rate exceeds the maximum linear growth rate. In Fig. 11(b), a very similar discharge but with the input power reduced slightly, there is no clear transition to the enhanced confinement regime, and $\omega_{E\times B}$ remains below $\gamma_{lin}^{max}$. The q profile for the cases shown in Fig. 11(a) and 11(b) are identical (Synakowski 1997b).

Also shown in Fig. 11 is a third observation in support of E×B shear stabilization of microturbulence: the density fluctuations decrease at the same time as the improvement in transport and when $\omega_{E\times B} > \gamma_{lin}^{max}$ in the example with no transition, there is no reduction in the turbulence (Mazzacato

1996, 1997). There is also a spatial correlation between the reduced transport and reduced turbulence observed. An example is the DIII–D NCS H–modes where the ion transport is reduced to near neoclassical levels across the entire discharge, and the density fluctuations are also reduced across the entire discharge cross section (Doyle 1996, Greenfield 1997, Burrell 1997).

A fourth observation in support of the E×B paradigm is that the local transition begins in the core of the discharge and propagates outward as predicted by Diamond (Diamond 1997). The transition begins first in the core because the growth rate of trapped particle modes is reduced there as a consequence of negative magnetic shear, Shafranov shift, $T_i/T_e >> 1$, and $n_i^{th}/n_e < 1$. In a number of cases the calculated growth rate can be near zero near the axis as seen in Fig. 9. The reduced transport region then moves radially outward until the E×B shearing rate can no longer overcome the instability. This beginning in the core and moving outward is shown clearly in examples from JET (Jones 1997) and JT–60U (Fujita 1996) in Fig. 12.

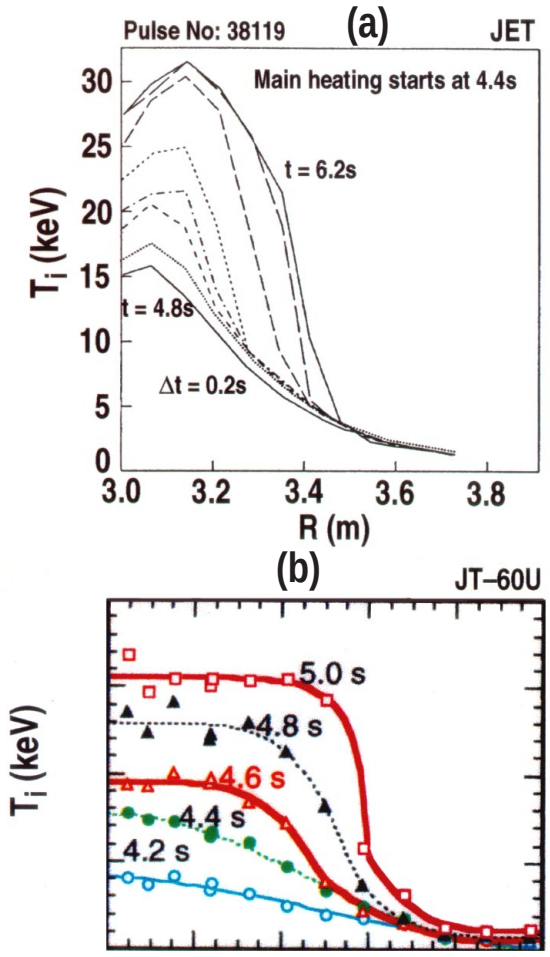


Fig. 12. Local transition starts first in the core and propagates outward (a) $T_i$ profiles from JET discharge JET [Jones, Phys. Plasmas 4, 1731 (1997)]; and (b) $T_i$ profiles from JT–60U discharge [Fujita, 1996 IAEA, Montreal, IAEA-CN-64/A1-4].

Finally, careful comparison of co to balanced to counter neutral beam heated discharges in TFTR show the importance of the sheared E×B in sustaining the reduced transport. The radial force balance gives $E_r = \nabla p/(enZ) + v_\phi B_\theta + v_\theta B_\phi$ where $\nabla p$ is the gradient of the pressure, e is the proton charge, n is the ion density, and Z is the ion charge number; $v_\phi$ and $v_\theta$ are the toroidal and poloidal fluid velocities, and $B_\phi$ and $B_\theta$ are the toroidal and poloidal magnetic fields. It is the radial electric field and the toroidal magnetic field that create the sheared E×B flow and as seen from above equation, the radial electric field is composed of a pressure gradient term and two flow terms. In TFTR balanced injection discharges, the plasma flow is small, and the pressure gradient dominates in the radial electric field and the sheared E×B flow. (This is in contrast to DIII–D co-injected discharges where $v_\phi B_\theta$ is the major contributor to the core radial electric field) For TFTR co-injected discharges, the toroidal rotation is in opposition to the pressure gradient term and the radial electric field is reduced. ERS discharges were formed with balanced injection in TFTR and then, with the total power held fixed, the co-counter mix was varied. The enhanced core confinement was sustained in the balanced and counter injection discharges. But, as the injected power was varied from balanced to co-, the enhanced confinement core was lost at an earlier time, consistent with the reduction in $E_r$ and sheared E×B (Zarnstorff 1996, Synakowski 1997).

Although the E×B shear explanation of the reduced transport does not involve the q profile directly, the q profile can impact the improved confinement in a number of ways. First there is a reduction in the growth rate of trapped particle modes at reduced magnetic shear and also at increased magnetic shear: for example see Fig. 2. Secondly, there is an increase in the Shafranov shift from the increase in the central q value (Beer 1997). The Shafranov shift alone could lead to a bifurcation, but this does not as yet seem to be the case in the experiments. Thirdly, there can be an increase in the E×B shearing rate in the negative shear regime as shown clearly by Synakowski (Synakowski 1997b). And finally in the region of vanishing shear, it is proposed that there is decorrelation of the turbulence as a consequence of the increased spacing between rational q values (Garbet 1997). So it is clear that in the experiments the q profile plays an important role in the formation of the internal transport barrier. And the importance of the q profile in the reduction of transport is not inconsistent with the sheared E×B flow paradigm. However, there are a number of observations not yet explained in the context of the sheared E×B paradigm.

In Tore Supra discharges heated by lower hybrid, with off axis current drive, an enhanced performance regime is observed (Litaudon 1996a, 1996b, 1997). This lower hybrid enhanced performance (LHEP)

regime is correlated with reversed q profile or a region of negative central shear. The reduced transport is observed in the electron channel and the more negative the magnetic shear, the larger the reduction in the transport, as is shown in Fig. 13. The results are for the quiescent phase of the discharges where the toroidal electric field is calculated to be constant and flat across the radius. The central plasma rotation in such discharges is of the order of 2–3 kHz and is not sufficient for E×B stabilization, and the ion pressure is also expected not to contribute significantly to E×B shear: the main mechanism for the improved electron confinement seems to be the weak or negative magnetic shear (Litaudon 1996a, 1996b, 1996c). These results indicate that the magnetic shear may play a larger role in the transport, especially the electron transport, than is indicated from sheared E×B only.

There are also some indications that the more negative magnetic shear may reduce ion transport. The ion transport was compared in two DIII–D NCS discharges. The shearing rate was larger than the maximum linear growth rate over almost exactly the same portion of the discharges, and the shearing rate and the maximum linear growth rates are both very similar for the two discharges. However, the discharge with the more negative magnetic shear had a significantly lower ion thermal transport. The different q profiles were obtained by different heating power during the current ramp as indicated in Fig. 6, and the heating power during the high power phase was the same. Sheared E×B flow alone is not sufficient to explain this difference in transport (Schissel 1996, Greenfield 1997).

The stabilization of mircoturbulence by sheared E×B flow is the leading explanation for the observed reduction in transport in NCS/RS/optimized shear discharges. Many of the observations are consistent with the theory. However, the observed dependence of the electron transport on the magnetic shear in Tore Supra, and the absence of any improvement in electron transport in other experiments is not easily explained. Also not easily explained is the reduction of ion thermal transport and particle transport to neoclassical levels, but the momentum transport remains much larger than neoclassical, although it is significantly reduced. It may be that sheared E×B stabilizes turbulence of large radial extent, but does not stabilize fine scale turbulence. Improvements in the gyrokinetic theory with fully nonlinear calculations including sheared E×B flow are needed.

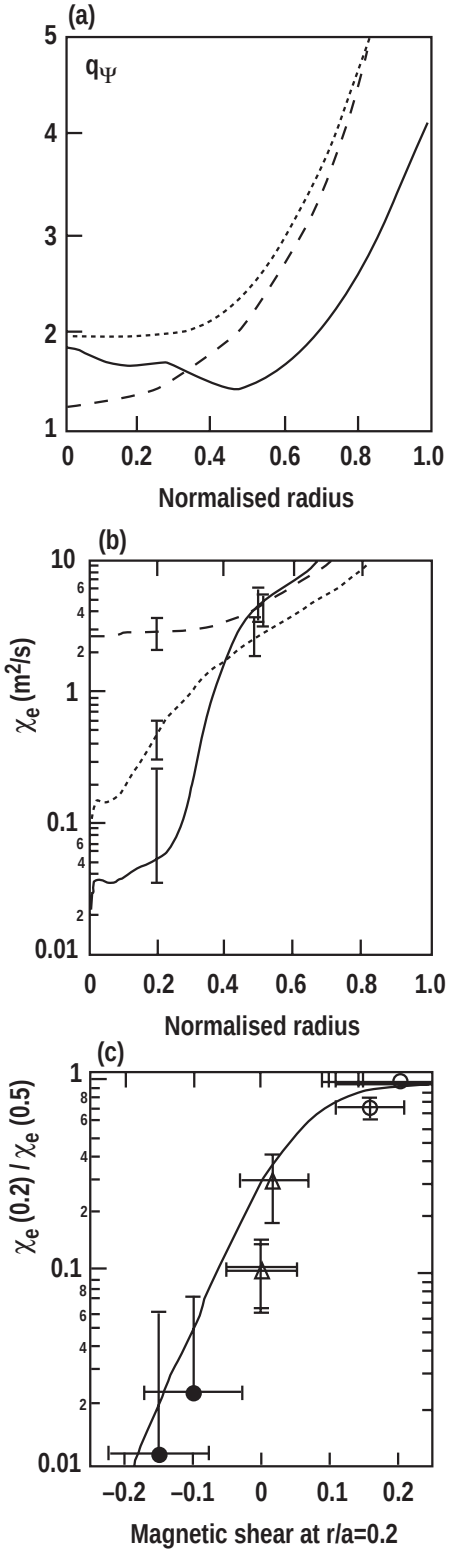


Fig. 13. Electron transport is observed to decrease with increasingly more negative magnetic shear in Tore Supra LHCD discharges (X. Litaudon, 1996 IAEA, Montreal). (a) q profile, (b) electron diffusivity profiles $\chi_e$, (c) ratio of electron diffusivity at r/a = 0.2 to electron diffusivity at r/a = 0.5.

## IV. Stability

Performance in these NCS/ERS/optimized shear discharges with an internal transport barrier and peaked pressure profiles is limited by disruptions near the calculated beta limit. Most of these disruptions in NCS/ERS/optimized shear discharges are very abrupt and rapid. An example of a DIII–D discharge is shown in Fig. 14 (Strait 1997). High power heating begins at 1.4 s and there is a near linear rise in the neutron emission until the disruption. Immediately prior to the disruption a rapidly growing n=1 perturbation is observed on the Mirnov coils. In almost all cases [DIII–D, TFTR (Fredrickson 1997), JT–60U (Koide 1997), and JET (Jones 1997)] the disruption precursor has toroidal mode number, n=1, and the growth time $\gamma^{-1}$ = 0.1–0.5 ms: in some JT–60U RS discharges disruption

precursors with $\gamma^{-1}$ = 0.1–0.5 ms have been observed. As shown in Fig. 14, the magnitude of the magnetic perturbation is very large, reaching $\tilde{B}_\theta/B_\theta$ (ave) $\gtrsim$ 10%. The disruption precursor also has a ballooning character, being much larger on the low field side than the high field side.

The most likely instability for the precursor leading to the termination of the NCS discharges is a n=1 ideal kink-ballooning, also sometimes referred to an infernal mode. The calculated mode structure for a TFTR discharge is shown in Fig. 15 and compared to the measured displacement (from electron cyclotron emission) (Fredrickson 1997, Manickam 1997) The mode is somewhat localized in the weak shear region, but there is significant radial displacement across the entire cross section. The toroidal mode number is n=1 and the poloidal structure is dominantly m=2 coupled to m=3. The mode is driven by high p′ in the region of low shear, near $q_{min}$. It is calculated to become unstable at lower values of beta near rational values of q, as is observed in the experiment: disruptions are often observed to occur as $q_{min}$ passes through rational values. In both TFTR and JT–60U, high beta NCS/RS discharges are not obtained with $q_{min} < 2$. Some discharges in DIII–D disrupt at beta values approximately 20% below the calculated ideal limit. These discharges are calculated to be unstable to a resistive interchange and are also unstable to a double tearing mode in the absence of plasma rotation. The strong rotational shear stabilizes the double tearing, but bursts of MHD, localized in the negative shear region and possibly a resistive interchange reduces the rotational shear and may drive the double tearing unstable (Chu 1995, 1996; Strait 1997).

A number of authors have calculated that the stability limit can be increased by a broadening of the pressure profile (Turnbull 1996, 1997; Phillips 1996; Bonoli 1997; Manickam 1994). The impact of the pressure profile on the ideal stability limit for a specific q profile and for a D-shape equilibria ($\kappa$ = 1.8, $\delta$ = 1.7) is shown in Fig. 16. It is noted that the maximum stable beta value, and normalized beta., $\beta_N$ are calculated to more than double as the pressure peaking factor, p(0)/⟨p⟩, goes from 6 to 3. Here p(0) is the pressure on axis, and ⟨p⟩ is the volume average pressure. Also shown in Fig. 16 is the resistive interchange limit, which has the same dependence as the n=1 ideal kink limit, but is approximately 20% to 25% lower. In DIII–D, the pressure profile can be broadened transiently by a controlled transition to H–mode during the NCS discharge (Lazarus 1996a, 1996b, 1997; Greenfield 1997). The trajectories of an L–mode NCS discharge and an H–mode NCS discharge are compared in Fig. 16(a). As can be seen the L–mode NCS begins to increase in beta and profile peaks: it disrupts near the calculated ideal limit. As the pressure profile broadens in the H–mode NCS, beta increases to $\beta_N > 4$, consistent with the stability calculations.

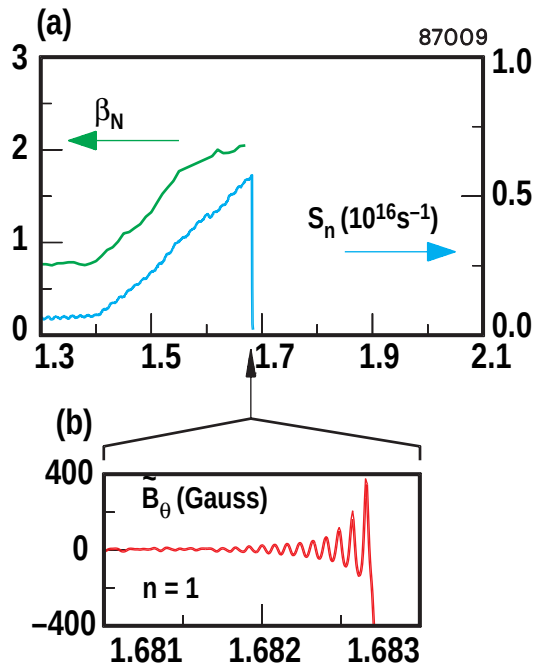


Fig. 14. Disruptions in NCS discharges with peaked pressure profiles limit performance (Chu 1996). (a) Temporal evolution of normalized beta and neutron emission, (b) expanded trace of precursor magnetic fluctuation.

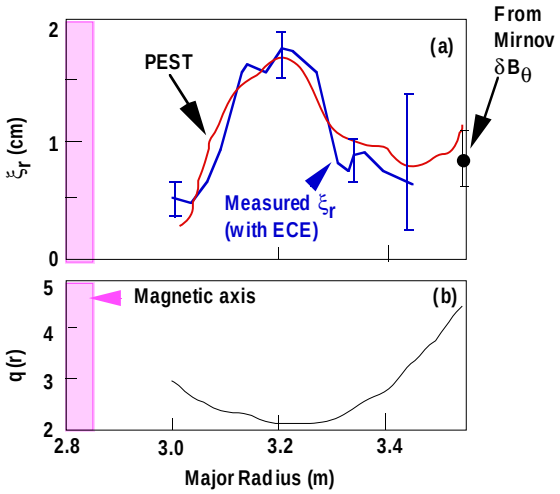


Fig. 15. Mode structure of disruption precursor agrees well with ideal stability calculations (Fredrickson 1997). (a) Perturbed displacement, (b) q profile.

It should be noted that the shaped NCS H–mode discharges do not normally reach high beta values implied in Fig. 16: stable beta value with $\beta_N$ up to 6 are calculated and MHD often limits $\beta_N$ to near or below 4. However, as in any ELM free H–mode, the transport near the boundary is very low leading to very steep pressure gradients, and the associated high bootstrap current near the boundary. This high pressure

gradient and edge current leads to n > 1 edge instabilities which most often terminate the high performance (Strait 1997, 1994b).

There is a synergistic effect in achieving high beta between the pressure profile and the plasma cross section shape. There is an increase in $\beta_T$, $\beta_N$, and $\beta_T^* = \langle p^2 \rangle^{1/2}\, 2\,\mu_0/B^2$, as one goes from a circular to a more strongly shaped (elongated and triangular) plasma, and there is an increase as the pressure profile becomes broader. These effects are shown together in Fig. 16(b). As can be seen, for the broad pressure profiles, $\beta_N$ is larger by a factor of 2 for the shaped plasma compared to the circular plasma: the rms beta, or $\beta_T^*$ (not shown), is larger by a factor of 5, and the fusion reactivity or fusion power is proportional to the $(\beta_T^*)^2$. Pressure profiles that are consistent with well aligned bootstrap current are broad pressure profiles, being near the left hand side in Fig. 16 (Turnbull 1997).

Wall stabilization is necessary to achieve high beta for the broad current density profiles and broad pressure profiles. The impact of the proximity of a wall to the plasma is shown in Fig. 17. As is seen for equilibrium shown, a factor of two in normalized beta is calculated for the actual DIII–D wall, compared to the value with no wall. Of course, a real wall is resistive and is expected to slow down the growth of the mode as opposed to stabilizing it completely. However, plasma rotation with respect to the wall is calculated to provide stability above the no wall limit (Bondeson 1994, Boozer 1995). Experiments on DIII–D have confirmed resistive wall stabilization for many resistive wall times (Strait 1995a, Taylor 1995). These experiments indicate that plasma rotation at the q = 2 and 3 surfaces of only 1 to 2 kHz is sufficient to maintain stability. It remains a key challenge for the advanced tokamak program to demonstrate resistive wall stabilization at beta values significantly beyond the no-wall value for long durations. Sustained plasma rotation and active non-axisymmetric feedback stabilization (Fitzpatrick 1996, Jensen 1997) are presently thought to be the means to meet this challenge.

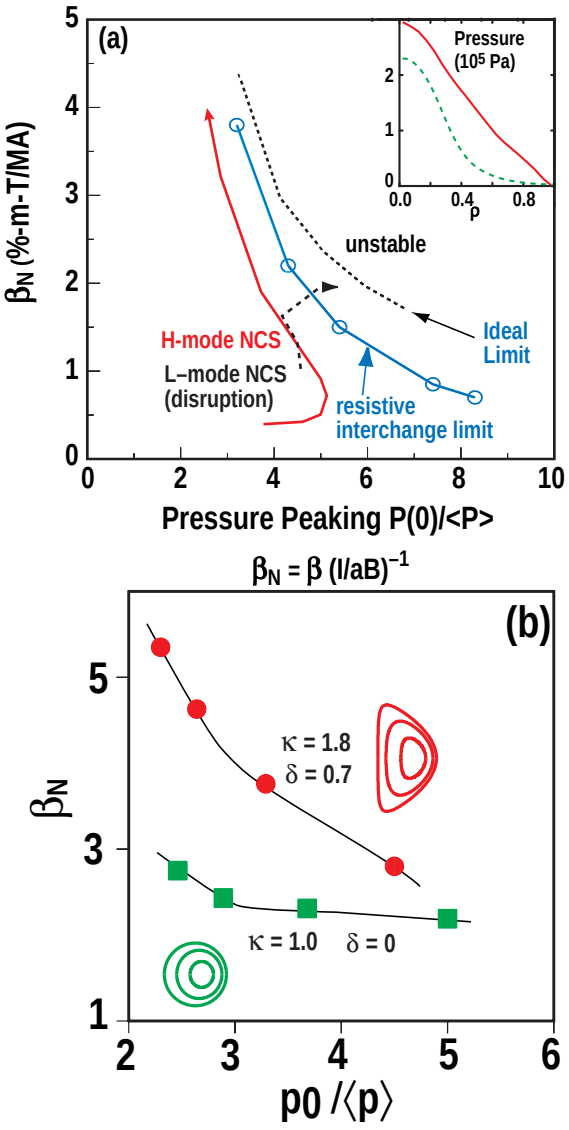


Fig. 16. Higher β is obtained with broad pressure profile (a) normalized beta vs. pressure peaking. Ideal and resistive limits are from generated equilibria similar to the experimental. Dashed trajectory is for an L–mode NCS discharge, solid trajectory is for H–mode NCS discharge (Lao 1996). Insets are exp. pressure profile just prior to disruption.(b) $\beta_N$ vs. pressure peaking for D shaped and circular shaped equilibria, $q_0 = 3.9$, $q_{min} = 2.1$, $q_{95} = 5.1$, rw/a = 1.5 (Turnbull 1996).

## V. Performance

The NCS/ERS/optimized shear regime has led to improved performance in several tokamaks; DIII–D, JET, and JT–60U. In DIII–D, the combination of strong cross section shaping ($\kappa = 2$, $\delta = 0.8$), q profile optimization (NCS), and pressure profile optimization (broad pressure with H–mode NCS) has led to more than a three-fold increase in neutron emission; the D-D energy gain, $Q_{DD}$; and equivalent D-T energy gain, $Q_{DT}^{EQ}$ (Lazarus 1996a, 1996b, 1997; Chan 1996; Schissel 1996; Greenfield 1997). A maximum neutron rate of $2.4 \times 10^{16}$/s and $Q_{DD} = 0.0015$ was obtained. Here the Q values are simply the neutron power emitted divided by auxiliary heating power. An equivalent D-T energy gain was calculated with TRANSP to be $Q_{DT}^{EQ} = 0.32$; with $\beta_T = 6.7\%$; $\beta_N = 4$%-m-T/MA; confinement time, $\tau_E = 0.4$ s; and confinement enhancement over L–mode, $H \gtrsim 4$. Performance improvement was also obtained in single-null divertor discharges with a plasma cross-section shape similar to that of JET and ITER, with $\beta_N = 4$ and H = 4, but with smaller energy gain as a consequence of the lower plasma current (Strait 1996).

The record D-D performance in JET was also obtained in the optimized shear regime. The discharge evolution is shown in Fig. 18. ICRF heating in the JET current ramp and flat top are critical in obtaining the best q profile and the high neutron yield. The ICRF is reduced following the formation of the internal barrier to avoid the stability limit. The discharge shown reaches $Q_{DD} = 0.0031$ and $0.6 < Q_{DT}^{EQ} < 0.8$, with $\tau_E = 0.4$ s and H = 2.2. The maximum D-D neutron rate was $5.6\times 10^{16}$/s. Although the q profile is not accurately measured, modeling and equilibrium analysis indicates that is nearly flat in the center to somewhat inverted (Gormezano 1997).

The record D-D performance in JT–60U was obtained in the reverse shear scenario, with a $Q_{DD} = 0.0047$, and $Q_{DT}^{EQ} = 1.05$. This calculation of Q takes into account the time rate of change in the stored energy, as well as alpha power and beam thermal power; $Q_{DT}^{EQ}$ (JT–60U) = $P_{DT}^{th}/(P_{aux} - dW/dt - P_{\alpha}^{th}) + P_{DT}^{b\text{-}th}/P_{aux}^{NB}$; where $P_{DT}^{th}$ is the calculated D-T fusion power from thermal D-T reactions, $P_{\alpha}^{th}$ is the calculated value of alpha heating due to thermal reactions, $P_{aux}$ is the total absorbed auxiliary power, $P_{DT}^{b\text{-}th}$ is the calculated fusion power from beam- thermal reactions, and $P_{aux}^{NB}$ is the absorbed neutral beam auxiliary power. The discharge evolution is shown in Fig. 19. Energy confinement is $\tau_E = 0.97$ s and H = 3.2. The discharge ends in a disruption at $\beta_N = 1.54$ near the calculated ideal limit. Note the very sharp gradient in the density, ion temperature, and electron temperature, a clear internal transport barrier, near the minimum in the q profile (Koide 1997).

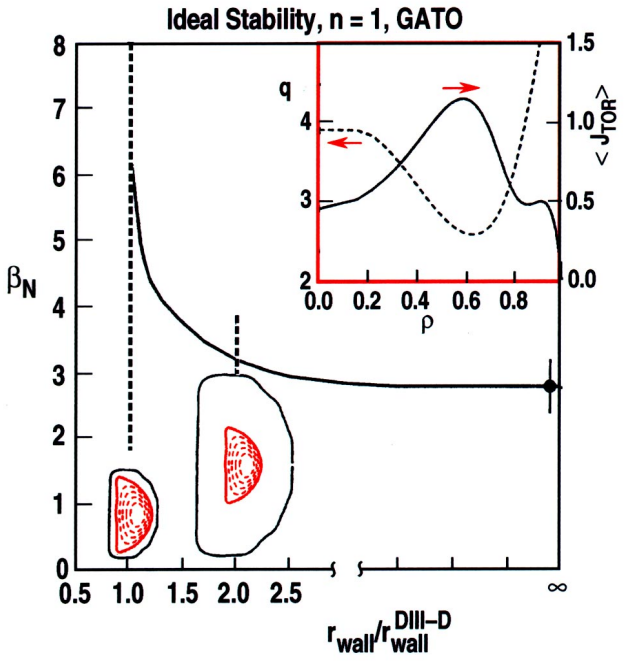


Fig. 17. Maximum stable beta increases for closer wall position: ideal n=1 stability using DIII–D plsma shape and DIII–D wall. Insets are typical current density and q profile (Taylor1995).

## VI. Progress Toward Steady State, Bootstrap Alignment

As just illustrated, the improvement in performance with NCS/ERS/optimized shear has occurred only transiently. The real challenge is to extend these improvements in confinement and stability toward steady state. Two of the features of the advanced tokamak regimes that require further evaluation and development to achieve steady state are: the (1) consistency of transport and resultant pressure profile and the pressure profile required for stability at high beta, and (2) alignment of the bootstrap current with total current profile required for stability and good confinement.

It is clear in the many experiments when turbulence is suppressed over a finite region, a local transport barrier is formed, and ion transport approaches neoclassical values, that the resultant steep local pressure gradient can lead to low n instabilities at modest values of beta. The VH–mode and ELM-free H–mode suffers from an edge instability as a consequence of the high edge pressure gradient which results from local transport barrier that is "too good." (Strait 1994b, 1997). The NCS regime, with only an internal transport barrier, also has problems with stability at modest values of beta because of the local high pressure gradient and pressure profiles that are too peaked. The NCS stability limit is improved by adding an H–mode edge, but these discharges, on the order of a confinement time after the H–mode transition experience similar edge instabilities as the VH–mode. It is expected that an NCS with an ELMing H–mode edge would have a pressure profile similar to that consistent with high beta calculations, but as of yet such a discharge has not yet been achieved at high beta. It seems very likely that some means to control the transport barrier (either the radial width or the extent of the transport reduction) may be needed to obtain the required pressure profiles. Experiments using rf to induce local electric fields has been attempted on TFTR, but without clear results.

A number of experiments have demonstrated that external current drive can maintain the reverse shear profiles in near steady state condition. Lower hybrid has been used both in JT–60U and Tore Supra to maintain the current profile in near steady state conditions (Ide 1996, Litaudon 1996, Ushigasa 1996). These examples were at modest values of beta, and maintaining the necessary current profile at high beta, with the corresponding high bootstrap current has not yet been demonstrated.

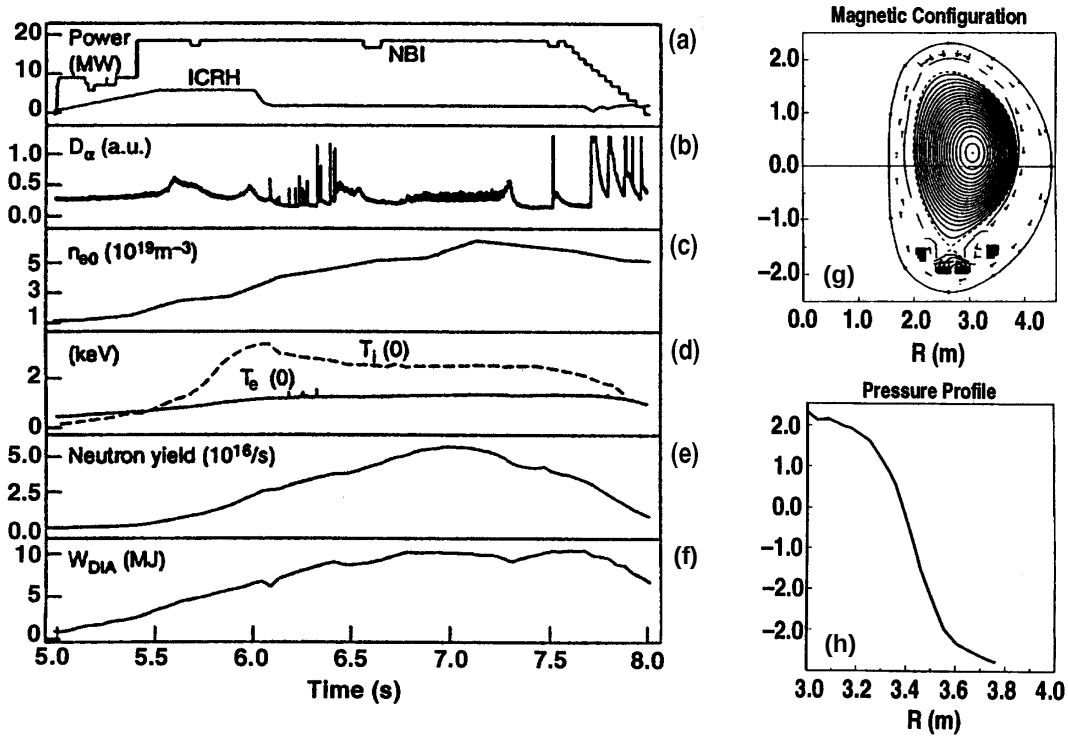


Fig. 18. Record DD JET performance is in optimized shear scenario (Gormezano 1997, Söldner 1997). (a) Neutral beam ICRH heating, (b) divertor $D_\alpha$ emission, (c) central electron density, (d) ion and electron temperature, (e) neutron yield, (f) plasma stored energy, (g) magnetic configuration (h) pressure profile.

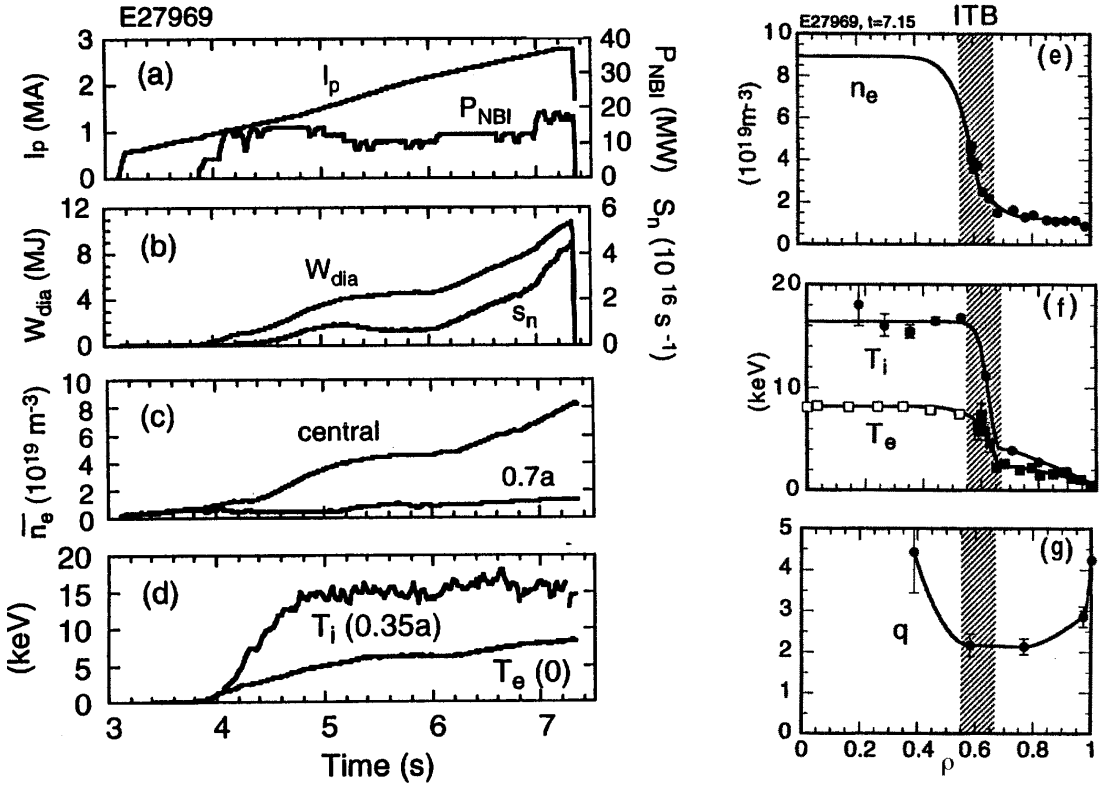


Fig. 19. Highest performance JT–60U reverse shear scenario (Koide1997). (a) plasma current and neutral beam heating power, (b) plasma energy and neutron emission, (c) electron density, (d) ion temperature, (e) electron density profile, (f) electron and ion temperature profiles, (g) q profile.

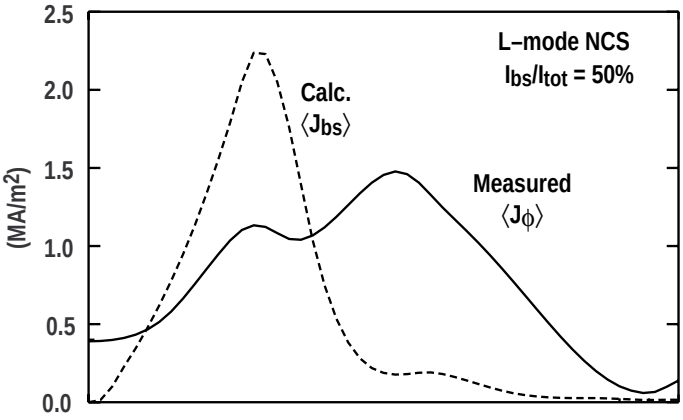


Fig. 20. Misalignment of bootstrap current with total current in DIII–D NCS discharge. Solid is measured total current, dashed is calculated bootstrap current from measured profile.

For an advanced tokamak scenario to be viable, the total current drive requirement must not be too large, else the gains realized with higher beta and higher confinement will be lost on the high recirculating power. Low current drive requirements lead to the need for reasonably high bootstrap current and good alignment of the bootstrap current and the total current. The mismatch between the target and bootstrap current for the high $\ell_i$ scenario has already been pointed out. The NCS regime, in principle could have much better bootstrap alignment, and is one of the attractive features of this regime. High beta well aligned bootstrap current equilibria have been found numerically (Kessel 1994, Manickam 1994, Turnbull 1995, St John 1995, Miller 1996). However, in experiments to date, the pressure gradient and resultant bootstrap is quite large at the internal transport barrier which normally lies inside the minimum in q; creating a misalignment between the bootstrap current and the total current, as is shown an example from DIII–D, in Fig. 20. This case shown is at $\beta_N = 2$ and $\beta_P = 1$, and the magnitude of the bootstrap would become larger and the misalignment more pronounced at higher beta. The alignment of the bootstrap current is predicted to improve with broader pressure profiles and larger radii of $q_{min}$ (Turnbull 1996). Self-consistent calculations indicate that high beta, high bootstrap current equilibria with the required alignment can be obtained with modest current drive assuming a fairly wide range of thermal diffusivity profiles (St John 1995). However, a narrow internal transport barrier where the pressure gradient is very steep over a narrow region especially an ITB in the density, is likely to produce an excess of bootstrap current and means to modify the barrier and or barrier width are likely needed.

## VII. Summary

Advances in physics can lead to more attractive compact tokamak power plants: 1) improved confinement, higher $H$; 2) improved stability, higher $\beta_N$; 3) steady state, high bootstrap fraction. High $\beta_N$ is a key to compact steady-state tokamaks. Investigations of three advanced tokamak scenarios and their advantages have been described.

- Radiative I–mode → reduced peak heat flux, high density, high confinement; possible limitation, $\beta_N$?
- High $\ell_i$ → robust high $\beta_N$ and $H$, compatible with RI–mode and ELMing H–mode; possible limitation, alignment of the bootstrap
- NCS, RS/ERS, optimized shear → improved bootstrap alignment (predicted); improved stability to trapped particle modes and ballooning mode, high $H$, high $\beta_N$; challenge, extend to steady state.

The improved confinement in these regimes is consistent with E×B sheared flow stabilization of microturbulence, especially in the NCS scenario. There are both spatial and temporal correlation amongst transport reduction, $\omega_{E\times B} > \gamma_{max}$, and stabilization of fluctuations. Transition begins in the core and moves outward as predicted. The reduction in $\chi_e$ with more negative magnetic shear may not be consistent with the paradigm, and may indicate a more important role of th q profile.

Beta limit in NCS discharges is a consequence of steep pressure gradient at the internal transport barrier (high $p_o/\langle p\rangle$. The beta limit is increased by broadening pressure profile, strong plasma shaping, and wall stabilization. Optimized magnetic shear has led to improved performance in JT–60U, JET, and DIII–D. Experiments carried out in DD plasmas indicate a $Q_{DT}^{EQ}$ of 1 in JT–60U, 0.6–0.8 in JET, and 0.3 in DIII–D.

A major challenge remains:to sustain steady-state, high-performance tokamak operation. Pressure profiles must be controlled through internal transport barrier control in order to obtain a good alignment of the bootstrap current with that needed to optimize the q-profile. While q-profile control has been demonstrated on JT–60U, Tore Supra, and JET using LHCD further work is needed to demonstrate sustaining these discharges at high $\beta$ with a high fraction of bootstrap current.

## ACKNOWLEDGMENT

This is a report of work supported by the U.S. Department of Energy under Contract Nos. DE-AC03-89ER51114, W-7405-ENG-48, DE-AC05-96OR22464, DE-AC02-76CH03073, and Grant Nos. DE-FG02-89ER53297, DE-FG02-91ER54109, and DE-FG03-86ER53266.

I would like to thank the following people for their contribution to this paper: K.H. Burrell, M. Beer, V.S. Chan, E.J. Doyle, J.R. Ferron, E. Fredrickson, T. Fujita, C. Gormezano, C.M. Greenfield, S. Ide, T.C. Jones, Y. Kamada, L.L. Lao, E.A. Lazarus, F. Levinton, Y.R. Lin-Liu, X. Litaudon, J. Manickam, A.M. Messiaen, D. Moreau, G.A. Navratil, J. Ongena, M. Porkolab, C.L. Rettig, G. Rewoldt, B.W. Rice, S. Sabbagh, D.P. Schissel, G.M. Staebler, F. Söldner, E.J. Strait, E.J. Synakowski, A.D. Turnbull, R.E. Waltz, G.H. Wolf, and M. Zarnstorff.

## REFERENCES

Beer M A, et al. 1997 *Phys. Plasmas* **4** 1792
Burrell K H, et al. 1997 *Phys. Plasmas* **4** 1499
Bonoli P T, et al. 1997 *Plasma Phys. and Contr. Fusion* **39** 223
Bondeson A, Ward D J 1994 *Phys. Rev. Lett.* **72** 2709
Chan V S, et al. 1997 *Plasma Phys. and Contr. Nucl. Fusion Research 1996 Montreal* (International Atomic Energy Agency, Vienna) to be published
Chu M S, et al. 1996 *Phys. Rev. Lett.* **77** 2710
Chu M S, et al. 1995 *Phys. Plasmas* **2** 2236
Davidson R C, et al. 1995 *Phys. Plasmas* **2** 2417
Doyle E J, et al. 1997 *Plasma Phys. and Contr. Nucl. Fusion Research 1996 Montreal* (International Atomic Energy Agency, Vienna) to be published
Ferron J R, et al. 1993 *Phys. Fluids B* **5** 2532
Fitzpatrick R, 1996 *Nucl. Fusion* **36** 1
Fredrickson E D, 1997 *Phys Plasmas* **4** 1589
Fujita T, et al. 1997a *Phys. Rev. Lett.* **78** 2377
Fujita T, et al. 1996 *Plasma Phys. and Contr. Nucl. Fusion Research 1996 Montreal* (International Atomic Energy Agency, Vienna) to be published
Fujita T, 1997b *Fusion Engineering and Design* (to be published)
Galambos J D, et al.,1995 *Nucl. Fusion* **35** 551
Garbet, X., this conference
Goldston R, 1994 *Plasma Phys. and Contr. Fusion* **36** B213
Gormezano C and the JET Team, 1996 *Plasma Phys. and Contr. Nucl. Fusion Research 1996 Montreal* (International Atomic Energy Agency, Vienna) to be published
Gormezano C., 1997 *Proc. 12th Top. Conf. on Radiofrequency Power in Plasmas Savannah*, to be published
Greenfield C M, et al. 1997 *Phys. Plasmas* **4** 1696
Greenwald M, et al. 1988 *Nucl. Fusion* **28** 2199
Groebner R J, 1993 *Phys. Fluids B* **5** 2343
Hugon M, et al. 1992 *Nucl. Fusion* **32** 33
Ide, S, 1996 *Plasma Phys. and Contr. Nucl. Fusion Research 1996 Montreal* (International Atomic Energy Agency, Vienna) to be published
Jardin S C, et al. 1997 *Fusion Engineering and Design*, (to be published)
Jensen T H and Fritzpatrick R, 1997 *Phys. Plasmas* **4** 2997
Joffrin E, Eur-CEA-FC-1553 (Tore Supra faraday rotation)
Jones T T C an d the JET Team, 1997 *Phys Plasmas* **4** 1725
Kamada Y, et al. 1996 *Plasma Phys. and Contr. Fusion* **38** 1387
Kamada Y, et al. 1994 *Nucl. Fusion* **34** 1605
Kesner J, 1993 *Phys. Fluids B* **5** 2325
Kesner J, 1994 "Attractive fusion reactor pressure status and the future," in *Tokamak Concept Improvement*, Varenna conference
Kessel C, 1994 *Phys. Rev. Lett.* **72** 1212
Koide Y, et al. 1997 *Phys Plasmas* **4** 1623
Lao L L, et al. 1993a *Phys. Rev. Lett.* **70** 3435
Lao L L, 1992 *Phys Fluids B* **4** 232
Lao L L, et al. 1996 Phys. Plasmas **3** 1951
La Haye R J, et al. 1995 *Nucl. Fusion* **35** 988
Lazarus E A, et al. 1985 *Nucl. Fusion* **25** 135

Lazarus E A, et al. 1992 *Phys. Fluids B* **4** 3644
Lazarus E A, et al. 1996a *Phys. Rev. Lett.* **77** 2714
Lazarus E A, et al. 1997b *Nucl. Fusion* **37** 7
Lazarus E A, et al. 1996b *Plasma Phys. and Contr. Nucl. Fusion Research 1996 Montreal* (International Atomic Energy Agency, Vienna) to be published
Lin Liu Y R, 1995 *Bull. Am. Phys. Soc.* **40**
Levinton F M, 1989 *Phys. Rev. Lett* **63** 2060
Levinton F M, 1995 *Phys. Rev. Lett* **75** 4417
Levinton F M, 1997 *Plasma Phys. and Contr. Nucl. Fusion Research 1996 Montreal* (International Atomic Energy Agency, Vienna) to be published
Litaudon X., et al. 1996a *Plasma Phys. Contr. Fusion* **38** A 251.
Litaudon X., et al. 1996b *Plasma Phys. Contr. Fusion* **38** 1603
Litaudon X., et al, 1996c *Plasma Phys. and Contr. Nucl. Fusion Research 1996 Montreal* (International Atomic Energy Agency, Vienna) to be published
Manickam J, et al. 1994 *Phys Plasm* **1** 1601
Manickam J, et al. 1997 *Plasma Phys. and Contr. Nucl. Fusion Research* (to be published) (Proc. 16th Int. Conf., Montréal, 1996) "MHD Stability Studies in Reversed Shear Plasmas in TFTR"
Mazzucato E, et al. 1996 *Phys. Rev. Lett.* **77** 3145
Mazzucato E. et. al. 1997 *Plasma Phys. and Controlled Nucl. Fusion Research 1996 Montreal* (International Atomic Energy Agency, Vienna) to be published
Messiaen A M, 1996 *Phys. Rev. Lett.* **77** 2487
Messiaen A M, 1997 *Phys. Plasmas* **4** 1690
Miller R L, et al. 1996 *Phys. Plasmas* **4** 1062
O'Rourke J. 1991 *Plasma Phys. and Contr. Fusion* **33** 289
Phillips M W, et al. 1996 *Phys. Plasmas* **3** 1673
Rewoldt G, et al. 1996 *Phys. Plasmas* **3** 4074
Rewoldt G, et al. 1997 *Phys. Plasmas* (to be published) “Microinstability properties of negative mangetic shear discharges in the Tomakak Fusion Test Reactor and DIII–D”
Rice B W, et al. 1996a *Phys. Plasmas* **3** 1983
Rice B W, et al. 1996b *Plasma Phys. Contr. Fusion* **38** 869
Rice B W, et al. 1996c *Nucl. Fusion* **36** 1271
Rice B W, et al. 1995 *Rev. Sci. Instrum.* **66** 373
Sabbagh S A, et al. 1996 *Plasma Phys. and Contr. Nucl. Fusion Research 1996 Montreal* (International Atomic Energy Agency, Vienna) to be published
Sauter O, 1997 *Phys. Plasmas* **4** 1654
Schissel D P, et al. 1996 *Plasma Phys. and Contr. Nucl. Fusion Research 1996 Montreal* (International Atomic Energy Agency, Vienna) to be published
Simonen T C 1992 *J. Fusion Energy* **11** 79
Söldner F X, et al. this conference
Soltwisch H 1986 *Rev. Sci. Instrum.* **57** 1939
Staebler G M, et al. 1997a *Nucl. Fusion* **37** 287
Strait E J 1994a *Phys. Plasmas* **1** 1415
Strait E J, et al. 1994b *in Proc. 21st European Conf. on Controlled Fusion and Plasma Physics* (European Physical Society, Petit-Lancy, Switzerland) Vol 18B, Part I, p. 242.
Strait E J 1995a *Phys. Rev. Lett.* **74** 2483 (1995)
Strait E J, et al. 1995b *Phys. Rev. Lett.* **75** 4421
Strait E J, et al. 1996 *Contr. Fusion and Plasma Physics 1996 Kiev* (European Physical Society, to be published)
Strait E J, et al. 1997 *Phys. Plasmas* **4** 1783
St John H, et al. 1995 *Plasma Phys. and Contr. Nucl. Fusion Research 1994 Seville* (International Atomic Energy Agency, Vienna) vol 3 p 603
Synakowski E J, et al. 1997a *Phys. Rev. Lett.* **78** 2972
Synakowski E J, et al. 1997b *Phys. Plasmas* **4** 1736
Taylor T S, et al. 1991 *Plasma Phys. and Contr. Nucl. Fusion Research 1990 Washington* (International Atomic Energy Agency, Vienna) vol 1 p 177
Taylor T S, et al. 1993 *Plasma Phys. and Contr. Nucl. Fusion Research 1992 Wurzburg* (International Atomic Energy Agency, Vienna) vol 1 p 167
Taylor T S, et al. 1994 *Plasma Phys. and Contr. Fusion* **36** B229
Taylor T S., et al. 1995 *Phys. Plasmas* **2** 2390
Troyon F, et al. 1984 *Plasma Phys. and Contr. Fusion* **26** 209
Turnbull A D, et al. 1995 *Phys. Rev. Lett.* **74** 718

Turnbull A D, et al. 1996 *Plasma Phys. and Contr. Nucl. Fusion Research 1996 Montreal* (International Atomic Energy Agency, Vienna) to be published
Turnbull A D, et al. 1997 (to be published) " Synergism Between Cross-Section and Profile Shaping in Beta Optimization of Tokamak Equilibria with Negative Central Shear"
Ushigusa K, et al. 1996 *Plasma Phys. and Contr. Nucl. Fusion Research 1996 Montreal* (International Atomic Energy Agency, Vienna) to be published
Waltz R E, 1996 *Plasma Phys. and Contr. Nucl. Fusion Research 1996 Montreal* (International Atomic Energy Agency, Vienna) to be published
Waltz R E, et al. 1995 *Phys. Plasmas* **2** 2408
Wesson J 1985
Wolf G H, et al. 1996 *Plasma Phys. and Contr. Nucl. Fusion Research 1996 Montreal* (International Atomic Energy Agency, Vienna) to be published
Wróblewski D, Lao L L 1993 *Rev. Sci. Instrum.* **63** 5140
Yushmanov P N, et al. 1990 *Nucl. Fusion* **30** 1999
Zarnstorf M 1993 *Plasma Phys. and Contr. Nucl. Fusion Research 1992 Wurzburg* (International Atomic Energy Agency, Vienna) vol 1 p 111
Zarnstorff M 1996 *Bull. Am. Phys. Soc.* **40** 1996